J. Sustain. Metall. (2016) 2:216–227
DOI 10.1007/s40831-016-0054-8

THEMATIC SECTION: LOW EMISSION STEELMAKING

Development of a Novel Flash Ironmaking Technology with Greatly Reduced Energy Consumption and CO_2 Emissions

Hong Yong Sohn[1] · **Yousef Mohassab**[1]

Published online: 21 April 2016

Abstract Despite the dominance of the blast furnace ironmaking process, increasing attention is being paid to the development of new technologies with lower energy consumption and CO_2 emissions. At the University of Utah, a novel flash ironmaking technology to meet these demands is under development. This technology eliminates the highly problematic cokemaking and pelletization/sintering steps by directly utilizing iron ore concentrate, which is currently produced in large quantities in North America and elsewhere. This transformative technology is expected to allow significant energy saving and reduced CO_2 emissions compared with the blast furnace process. It has been demonstrated that iron of more than 95 % metallization can be obtained by reduction with hydrogen or a mixture of carbon monoxide and hydrogen in 2–7 s at temperatures of 1473–1823 K. The development of the technology has gone through the stages of proof-of-concept and small laboratory flash reactor tests. A large prototype bench reactor that has most of the features of an eventual industrial reactor has been commissioned. In this paper, some details of advances made in the development are discussed.

Keywords Flash ironmaking · Green technology · Iron ore concentrate · Kinetics · Slag

The contributing editor for this article was Sharif Jahanshahi.

✉ Hong Yong Sohn
h.y.sohn@utah.edu

Yousef Mohassab
yousef.mohassab@utah.edu

[1] Department of Metallurgical Engineering, University of Utah, 135 South 1460 East, Room 412, Salt Lake City, UT 84112, USA

Introduction

Despite the dominance of the blast furnace ironmaking process, increasing attention is being paid to the development of new technologies with lower energy consumption and CO_2 emissions. It should also require much less capital investment than the blast furnace/coke oven combination. At the University of Utah, an alternative technology to meet these demands, called the flash ironmaking technology (FIT), has been under development [1–7]. This novel technology eliminates the highly problematic cokemaking and pelletization/sintering steps by directly utilizing iron ore concentrate, which is currently produced in large quantities in North America and elsewhere. In this article, recent advances on this work are discussed.

The FIT is an innovative process that uses iron ore concentrate directly without further treatment. The fineness of the concentrate particles allows a very rapid reaction rate, thus requiring residence times measured in seconds instead of the minutes and hours it takes to reduce pellets and even iron ore fines.

Other processes for the gaseous reduction of iron oxide can be grouped into two broad types: (1) shaft furnaces (Midrex [8] and Energiron [9]), and (2) fluidized-bed reactors (FINMET and the earlier FIOR [10], CIRCORED Process [11], and SPIREX [12]). Shaft furnaces require pellets or sinter, which are of 10–12-mm size and require minutes or even hours to be fully reduced. The fluid-bed processes use "iron ore fines," i.e., particles in the range of +0.1 mm to −10 mm. These processes are slow because the larger pellets and particles react slowly, and the process cannot be operated at high temperatures, under which they suffer the problems of sticking and fusion of particles. Processes that can replace the blast furnace must be sufficiently intensive to meet the large production rates required for economic competitiveness. The FIT reduces iron ore concentrates of <100-μm sizes, which are smaller than fines by one or two orders of magnitude. Historically, fluidized-bed processes using iron ore fines have been less than successful. Compared with concentrate particles, even ore 'fines' used in a fluidized-bed process take much longer time to reduce than the time available in a typical flash reduction process.

The FIT removes many of the limitations associated with the other processes discussed above. Specifically, (1) it uses iron oxide concentrates directly without the need for pelletization or sintering; (2) coke ovens are not required; (3) high temperatures can be used because there will be little particle sticking or fusion problems (and thus, the process can be operated at high temperatures); (4) it is possible to produce either solid or molten iron; and (5) the raw materials can be fed continuously. The process also has the possibility of direct steelmaking in a single unit, as depicted in Fig. 1.

In this paper, we will describe major progresses made so far on the Flash Ironmaking research, especially the kinetics of the reduction process, the chemistry of the slag, and the economic and environmental aspects of the process.

Reduction Kinetics

Previous research on the gaseous reduction of iron oxide has typically involved samples larger than concentrate particles, such as ore fines and pellets as well as temperature ranges substantially lower than in the new flash ironmaking process. Ray and Kundu [13] reduced hematite in $CO–N_2$ mixtures in the temperature range 1073–1273 K (800–1000 °C) and determined an activation energy of 90 kJ/mol. Edstrom [14] studied the reduction of natural hematite crystals by hydrogen below 1273 K (1000 °C) and found that the hematite crystal swelled at first, but shrunk during the later stages when reduced by hydrogen. Hematite particles of 105–140-μm sizes were reduced by hydrogen in a silica-tube fluidized-bed reactor by Srinivasan and Sheasby [15] in the temperature range of 923–1173 K (650–900 °C). They found that a pore-free magnetite layer was formed adjacent to the hematite phase, but the magnetite layer developed porosity with further reduction. Piotrowski et al. [16] reduced hematite particles of 91-μm average size to wustite by carbon monoxide at 973–1173 K (700–900 °C). The nucleation-and-growth kinetic model was applied to the initial stages of the reduction process, which gradually shifted to diffusion control as reduction proceeded. They determined activation energy to be 58 kJ/mol. Sturn et al. [17] found that the phase boundary reaction was the most likely rate-controlling step for the reduction of hematite particle of 177-μm diameter by hydrogen in the temperature range 673–803 K (400–530 °C). Fruehan et al. [18] investigated the reduction of hematite particles of 180–250-μm size by hydrogen in the temperature range 873–1273 K (600–1000 °C) and found that a shell of dense iron formed around the wustite grains that significantly slowed the reduction rate, limited by the diffusion of oxygen atoms through solid iron when the grains were larger than 2 μm. Recently, Monazam et al. [19] studied the reduction kinetics of hematite (average size of 200 μm) to wustite with hydrogen at temperatures of 973–1223 K (700–950 °C). They reported that the reduction process can be divided into two stages: an induction period, and a nucleation-and-growth period. The induction period became shorter and the entire reduction process could be considered as nucleation/growth period at higher temperatures of 1123–1223 K (850–950 °C) with an apparent activation energy of 64 kJ/mol.

There has been previous work on the reduction of fine iron ore particles; but most of it has been performed at temperatures lower than 1273 K (1000 °C), because the existing gaseous reduction processes operate at lower temperatures than in the new flash ironmaking process, which is expected to be operated at a temperature above 1500 K.

There had been little work on the gaseous reduction of iron oxide concentrates under the conditions of the new flash ironmaking technology [1, 20, 21]. In conjunction with the development of the new process, Sohn and coworkers [1, 20, 21] have investigated the gaseous reduction of magnetite concentrate particles. Their work included the measurement of the intrinsic kinetics of the hydrogen reduction of magnetite concentrate particles in the temperature range of 1423–1673 K (1150–1400 °C) [1]. Most importantly, they have established that magnetite concentrate can be reduced to a degree higher than 90 pct within several seconds, which presents sufficiently rapid kinetics for a flash reduction process.

As an integral part of the development of this novel process, Sohn and coworkers [1, 22, 23] have determined detailed kinetics of the gaseous reduction of magnetite concentrate particles, aimed at generating a database to be used for the design of a flash ironmaking reactor; before

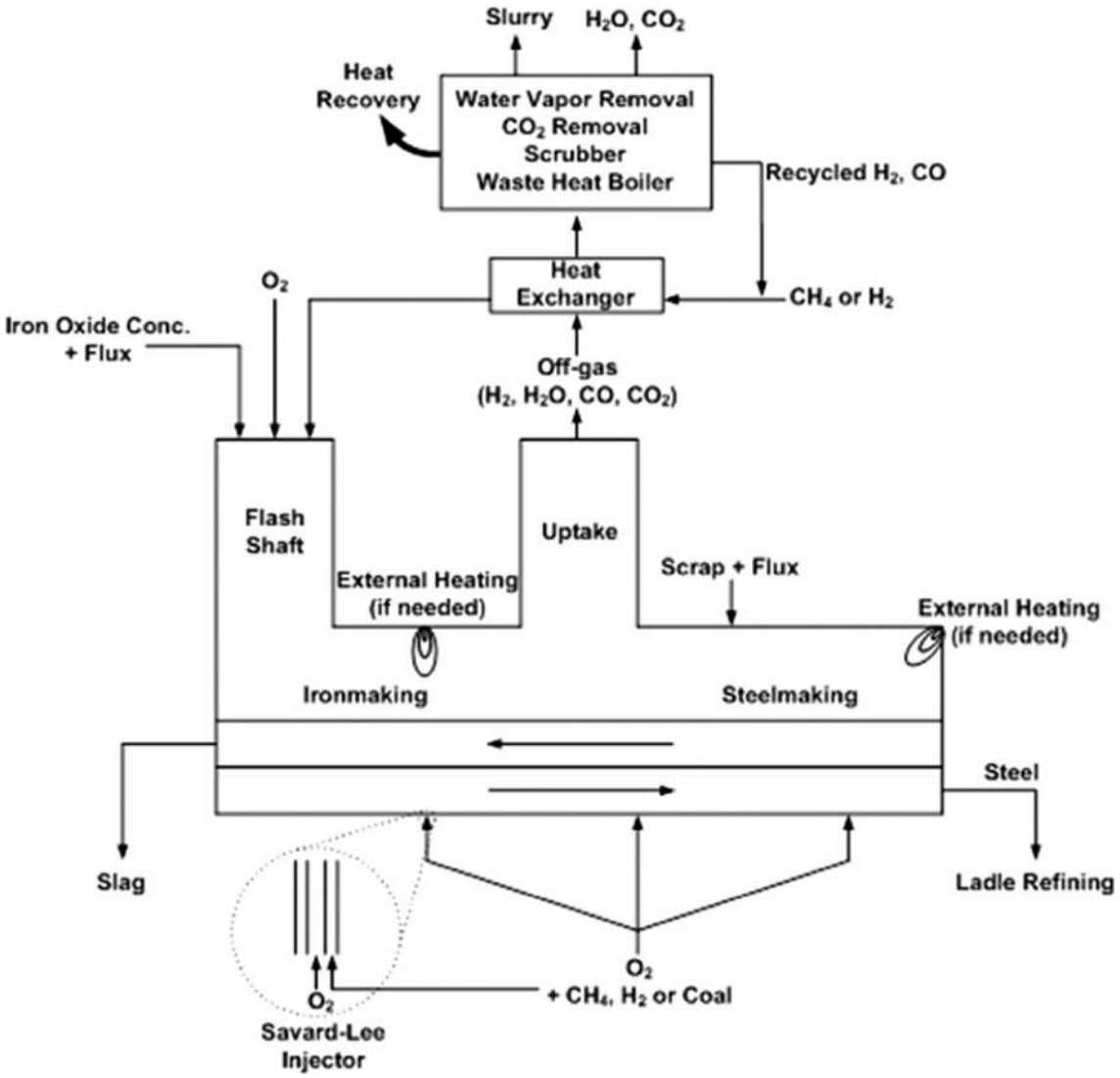

Fig. 1 A schematic diagram of a possible direct steelmaking process based on the Flash Ironmaking Technology (FIT) [61]

their work, there had been little research reported on this subject under the conditions of the FIT.

A number of kinetic equations were tested on the obtained experimental data to determine the best-fitting equation: the power law, contraction models, kinetics-order models, and the nucleation-and-growth model. From a mechanistic point of view, it is not uncommon in the gaseous reduction of very fine metal oxide particles to follow the nucleation-and-growth process. Supported by the goodness of the fit as well as the SEM micrographs shown in Fig. 2, the nucleation-and-growth model best represented the kinetics of hematite concentrate reduction by hydrogen. In the nucleation-and-growth kinetics, hydrogen is adsorbed on active sites on the surface and then reacts with oxygen and produces Fe nuclei that grow with time, as shown in Fig. 3. For small particles, the period of the formation and the growth of nuclei occupy essentially the entire conversion range. The reduction of hematite to iron in the temperature range of this work proceeds through the formation of Fe_3O_4 and FeO with changes in reactivity. However, for small particles, it is extremely difficult to follow the irregular evolution of morphology involving Fe_3O_4 and FeO formation and the overlapping regions of different reduction extents. Furthermore, the reduction of Fe_2O_3 to FeO accounts for only the first 33 % of conversion, whereas the main interest in this work and the new ironmaking technology is the attainment of much higher degrees of reduction. Thus, the following global nucleation-and-growth rate equation for the overall reduction process is appropriate:

$$[-Ln(1-X)]^{1/n} = [k \cdot f_p(pH_2, pH_2O)] \cdot t = k_{app} \cdot t \qquad (1)$$

where X is the fractional reduction degree; t is the residence time; n is the Avrami parameter [24–26]; k is the

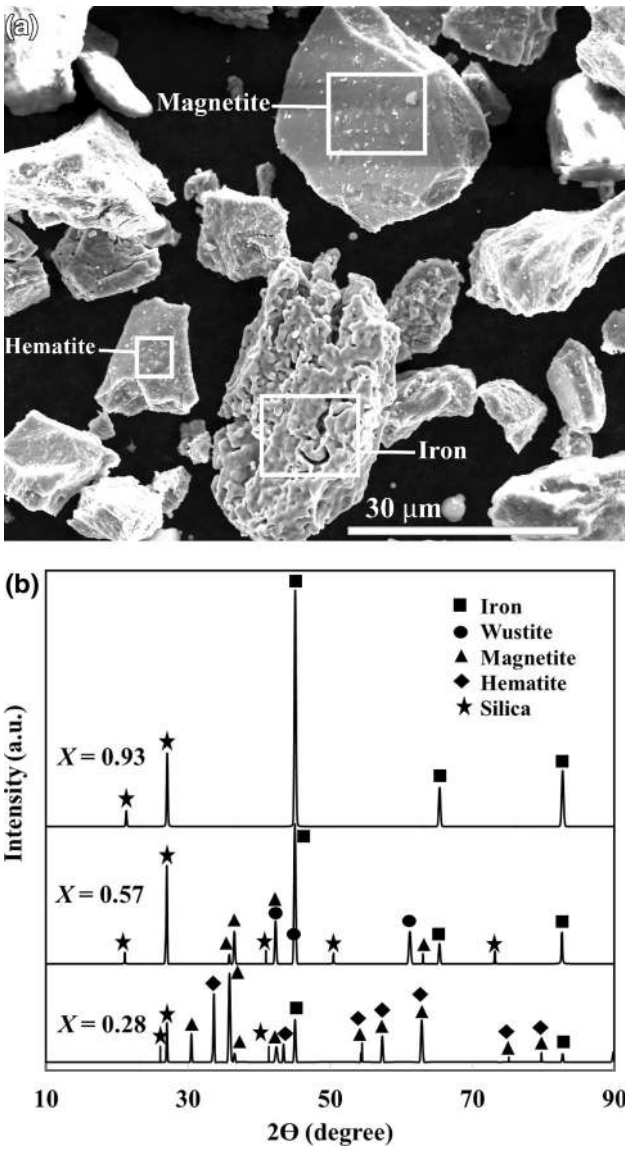

Fig. 2 Coexistence of various iron oxide phases along with iron as evidenced by **a** SEM micrographs of reduced sample particles ($X = 0.14$); and **b** XRD of samples with different reduction degrees [23]

rate constant; pH_2 and pH_2O are the partial pressures of hydrogen and water vapor, respectively; $f_p(pH_2, pH_2O)$ is the concentration driving force; and k_{app} is the apparent rate constant. Sohn et al. [1, 20, 22, 23] measured the kinetics of the reduction of magnetite or hematite concentrate particles by hydrogen or carbon monoxide in the temperature range of 1423–1673 K (1150–1400 °C). They obtained the following rate expression for the hydrogen reduction of magnetite concentrate particle in the temperature range of 1423–1623 K (1150–1350 °C) given by:

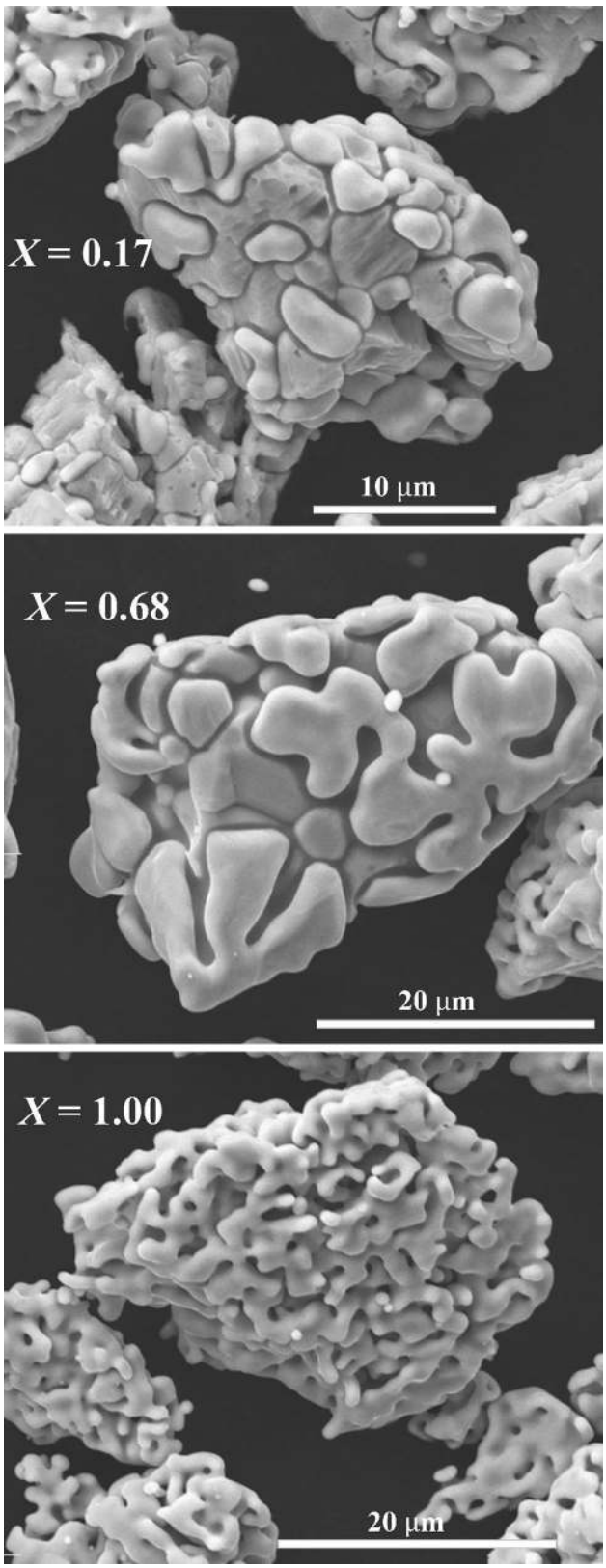

Fig. 3 SEM micrographs of hematite samples with different reduction degrees in the temperature range of 1473–1623 K (1200–1350 °C) with pH_2 ranging from 0.1 to 0.4 atm [23]

$$-Ln(1-X) = 1.23 \times 10^7 \times e^{\frac{-196{,}000}{RT}} \times \left(pH_2 - \frac{pH_2O}{K}\right)_{lm} \times t \quad (2)$$

where R is 8.314 J mol^{-1} K^{-1}, p is in atm, t is in seconds, and K is the equilibrium constant for the reaction: $Fe_{0.947}O + H_2 = 0.947\ Fe + H_2O$. It was shown previously [20] that a logarithmic mean (lm) between the input and the off-gas values appropriately represents the average hydrogen driving force for first–order dependence with respect to pH_2, and an arithmetic mean (am) is the appropriate average driving force for a half-order reaction.

Although the FIT is being developed for magnetite concentrate, it is expected to be equally applicable to hematite concentrate. Thus, Sohn and coworkers [23] studied the hydrogen reduction kinetics of hematite concentrate particles of average size 21 μm in the temperature range of 1423–1623 K (1150–1400 °C). The results clearly indicated that the hematite concentrate can also be reduced to greater than 90 pct degree by hydrogen in the several seconds of residence time typically available in a flash reactor. In their work [23], results at various temperatures and partial pressures of hydrogen showed that the nucleation-and-growth rate equation with an Avrami parameter of 1 well describes the kinetics of hematite reduction. The reduction rate has a 1st-order dependence on the partial pressure of hydrogen. The activation energy of hydrogen reduction of hematite concentrate is 214 kJ/mol [23]. The following rate equation was obtained, which satisfactorily represent the reduction kinetics of hematite particles:

$$-Ln(1-X) = 4.41 \times 10^7 \times e^{\frac{-214{,}000}{RT}} \times \left(pH_2 - \frac{pH_2O}{K}\right)_{lm} \times t \quad (3)$$

where R is 8.314 J/mol K, T is in K, p is in atm, and t is in seconds.

Compared with the activation energy for the hydrogen reduction of magnetite concentrate of 196 kJ/mol in the temperature range 1423–1673 K (1150–1400 °C), the reduction of hematite concentrate has a similar activation energy of 214 kJ/mol in the similar temperature range.

Hematite reduction kinetics by CO + H_2 mixtures was also investigated to represent the case of using natural gas or coal gas as the reductant/fuel in the flash ironmaking process [27]. The kinetics in this case is complicated due to the simultaneous reduction by the two reductants. It was found, however, that within a few seconds of residence time, a reduction degree of over 90 pct was achieved using CO + H_2 at temperatures above 1573 K (1300 °C), as shown in Fig. 4. It is also clear that adding CO to the H_2 boosts the reduction kinetics as compared with the reduction by a single gas H_2 or CO. Increasing CO partial pressure from 0.05 to 0.2 atm while holding hydrogen partial pressure at 0.2 atm did not affect the reduction kinetics of hematite concentrate, as Fig. 4 shows. The measurement of the kinetics of the flash reduction is continuing in order to determine the rate equation for the reduction of magnetite and hematite concentrate with mixtures of CO and H_2 to be used in designing a flash reactor that will run on natural gas.

Meanwhile, Sohn et al. [28, 29] studied the kinetics of the re-oxidation of iron particles produced by the FIT in various oxidizing gas mixtures. As the gas–particle mixture cools down in the lower part of the flash reactor, the re-oxidation of iron could take place because of the decreasing equilibrium constant and the high reactivity of the freshly reduced fine iron particles. The last stage of hydrogen reduction of iron oxide, i.e., the reduction of wustite, is significantly limited by equilibrium. The effects of temperature [823–973 K (550–700 °C)] and H_2O partial pressure (34–86 kPa) on the re-oxidation rate were examined. The nucleation-and-growth model was shown to best describe the re-oxidation kinetics. Pressure dependence was of first order with respect to water vapor, and the activation energy was 146 kJ/mol. A complete rate equation that adequately represents the experimental data was developed [29]. They also studied the oxidation in pure CO_2 gas in the temperature range of 873–1073 K (600–800 °C). Their findings indicated that within the several seconds of residence time typically available in a flash reduction process the re-oxidation degree of iron particles in water vapor should be <0.24 % in the temperature range of 823–973 K (550–700 °C) and the results implied that the oxidation will be negligible in the flash reduction process where CO_2 from partial combustion of natural gas with oxygen accounts for less than 10 % in the

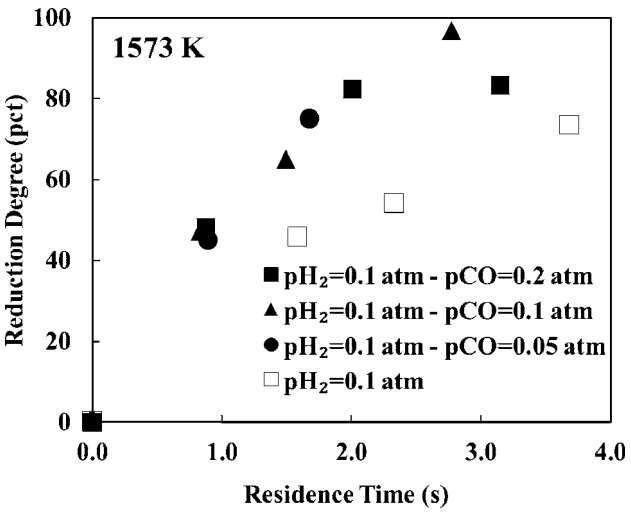

Fig. 4 Reduction degree comparisons between single reductant gas (H_2) and CO + H_2 mixtures at 1573 K (1300 °C) (adapted from [27])

gas mixture. In the collector where product iron particles may be kept for up to 1 h at around 673 K (400 °C), the expected re-oxidation degree would be around 0.02 % [28–30]. This indicates that re-oxidation within the reactor due to the shift in equilibrium as temperature decreases toward the bottom of the reactor is of no concern.

The pyrophoricity of direct reduced iron when it comes into contact with air is of concern during storage or transportation. Thus, oxidation of flash-reduced iron in O_2–N_2 gas mixtures was investigated to determine the effects of temperature [673–873 K (400–600 °C)] and O_2 partial pressure (3.4–18 kPa). The rate data were analyzed based on the nucleation-and-growth model, which resulted a pressure dependence of first order with respect to oxygen and an activation energy of 14.4 kJ/mol [28]. Most importantly, it was concluded that flash-reduced iron is much less vulnerable to oxidation than conventional direct reduced iron particles. This is because the flash ironmaking process uses higher reduction temperatures, leading to a lower specific surface area of the product iron. This can be clearly seen from the micrographs presented in Fig. 5, which shows iron oxide reduced at a lower temperature at which conventional DRI is produced (Fig. 5a) compared with iron produced at a flash ironmaking temperature (Fig. 5b). This work determined that at temperatures lower than 573 K (300 °C), the oxidation of flash-reduced iron is not of great concern [28]. In addition, Sohn and coworkers have developed a relationship between the fractional oxygen content (F) and time [29]:

$$\left[Ln\left(\frac{1-F_0}{1-F}\right)\right]^{1/1.26} = 941.5 \cdot \exp\left(-\frac{146000}{\mathrm{RT}}\right) \cdot (p_{\mathrm{H_2O}} - p_{\mathrm{H_2}}/K) \cdot t \quad (4)$$

where F_0 is the initial fractional oxygen content; K is the equilibrium constant of oxidation of iron to wustite [or magnetite less than 833 K (560 °C)] by $H_2O(g)$; T is in K; p is the pressure in kPa, and t is the time in seconds. Also, they developed a rate equation for the re-oxidation of flash-reduced iron particles in O_2–N_2 gas mixture as follows [28]:

$$Ln\left(\frac{1-F_0}{1-F}\right) = 0.006 \exp\left(-\frac{14,400}{\mathrm{RT}}\right) \cdot p_{\mathrm{O_2}} \cdot t \quad (5)$$

where F is the fractional oxygen content; R is the gas constant in J/mol K; p_{O_2} is the partial pressure of oxygen in kPa; and t is the time in seconds.

Slag Chemistry

Slag is one of the key components that determine the quality of iron produced during a smelting process. The capacity of the slag to absorb elements such as sulfur and phosphorus is mainly controlled by its composition together with oxygen potential and temperature. For instance, high basicity of the slag increases its sulfide capacity. Further, the slag chemistry has a strong impact on the activity of FeO in the slag, which impacts the yield at the end of ironmaking and steelmaking. It is important to understand how the slag chemistry and structure affect slag–metal reaction equilibria as well as slag properties such as viscosity, density, and conductivity. Ironmaking slags contain silica and other complex-forming components, and the structure of the silicate has a significant effect on the structure and behavior of the slag. In this laboratory, the effects of CO/CO_2, H_2/H_2O, and $CO/CO_2/H_2/H_2O$ gas atmospheres on the chemistry and structure of ironmaking slag were determined. Little work on slag chemistry under H_2–H_2O atmosphere had previously been reported in the literature. The results of this work are important in the development of an ecofriendly, novel, flash ironmaking process with the potential for steelmaking

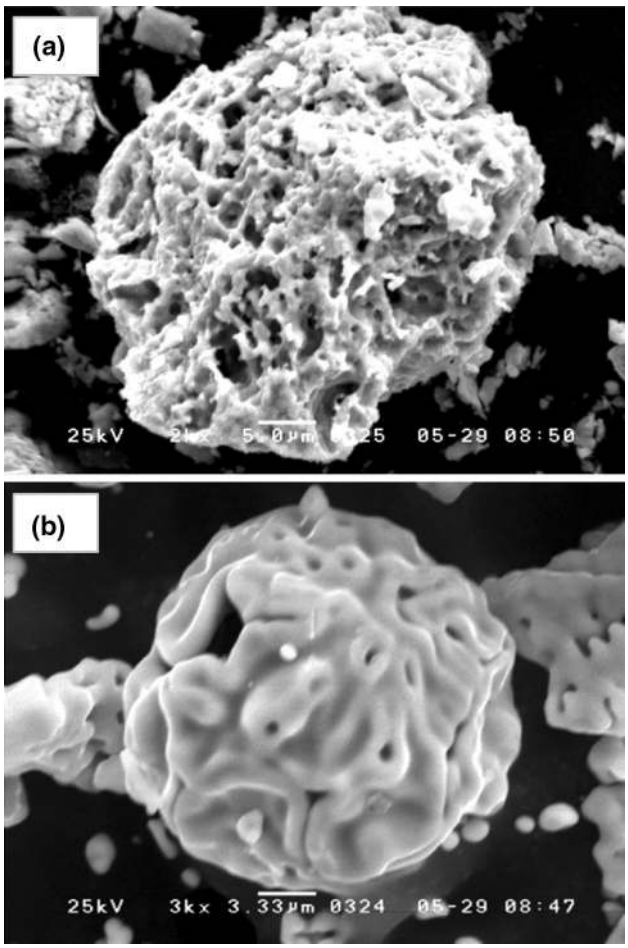

Fig. 5 Comparison of microstructures of different iron particles: **a** H_2-reduced iron at 1073 K (800 °C); **b** flash-reduced iron produced at 1623 K (1350 °C) [28]

in a single continuous process [1, 6, 7, 22, 23]. The solubility of water in various slags has been studied by many researchers [31–41]. In this work, the effects of the water vapor on the equilibrium distribution of elements such as sulfur [42, 43], phosphorus [7, 42], and manganese [44] in addition to the effects on the activities of iron and magnesium oxides were investigated [6, 45, 46].

In slag, silicate anions are composed of silicon cations surrounded by four oxygen anions forming tetrahedral units. These tetrahedra are joined together in chains or rings by bridging oxygen (BO), as shown in Fig. 6. Cations are classified into two categories with respect to their impact on the silicate chains or rings (silicate polymer): the first type is the network breaker where the cations tend to break the BO bond to form nonbridging oxygen (NBO): O^- and free oxygen, O^{2-}. This process is called depolymerization of silicate melt, which is usually expressed by the ratio of nonbridging oxygen atoms to the number of tetrahedrally coordinated atoms, or simply denoted as NBO/T ratio [47]. It is worth noting that the rates and equilibria in slag–metal reactions as well as the physical properties of slag are strongly dependent on the NBO/T ratio [48, 49]. Examples of the network breaker cations are Ca^{2+}, Mg^{2+}, and Fe^{2+}. In addition to this ratio, Si anions are frequently classified by the term structon or Q-notation (Q^n where n = 0, 1, 2, 3, and 4) which was defined as single atom (or ion or molecule) surrounded by others in a specified manner [50, 51]. Figure 6 shows examples of silicate ions with their Q-notation and NBO/T ratios in addition to other distinguishing features. A Si polyanion may have more than one isomer with different Q values, as will be shown subsequently.

The second type of cations is the network former such as Al^{3+} and P^{5+} which form AlO_4^{5-} and PO_4^{3-} units. To balance the electrical charge, cations such as Ca^{2+}, Mg^{2+}, or Fe^{2+} are required. The cations involved in charge-balancing duties do not participate in network breaking. Thus, Al_2O_3 increases the polymerization of the silicate melt [49]. Like Al_2O_3, P_2O_5 increases polymerization since it forms phosphate complexes that have greater affinity for cations, which are mostly of the network modifier type than silicate ions. This affinity toward cations accounts for the ability of phosphate to increase silica polymerization since phosphate consumes the silicate network modifiers and decreases the attack of these cations on the silicate polymers. It is noted that P_2O_5 is less likely to form P–O–Si bonds compared with the aforementioned phosphate complexes that are based on the PO_4^{3-} units [49].

The silicate melts comprise various 3-dimensionally interconnected units such as SiO_2, $Si_2O_5^{2-}$, $Si_2O_6^{4-}$, $Si_2O_7^{2-}$, and SiO_4^{4-} coexisting in the melt [49]. The nature of these units is affected by the nature of the cation in the silicate melt. The SiO_2 and SiO_4^{4-} units are stabilized by small cations of high valences, e.g., $Mg^{2+} > Ca^{2+} > Na^+$. In the presence of these basic metal oxides, silicate polymers are broken according to the following pattern: $Si_6O_{18}^{12-} \rightarrow Si_4O_{12}^{8-} \rightarrow Si_3O_9^{6-} \rightarrow Si_2O_7^{6-} \rightarrow SiO_4^{-4}$. This explains the absence of isolated SiO_2 molecules in industrial slags. Instead, SiO_2-based slags are known to consist of polymers of tetrahedral units (SiO_4^{-4}) [48, 52, 53].

Mohassab and Sohn [7, 43–46, 54, 55] have applied a number of analytical techniques to determine the structures and properties of the slags formed under the conditions of flash ironmaking. Several features of such instrumental analysis have direct correlations with important properties of slag such as its affinity to impurities. These techniques

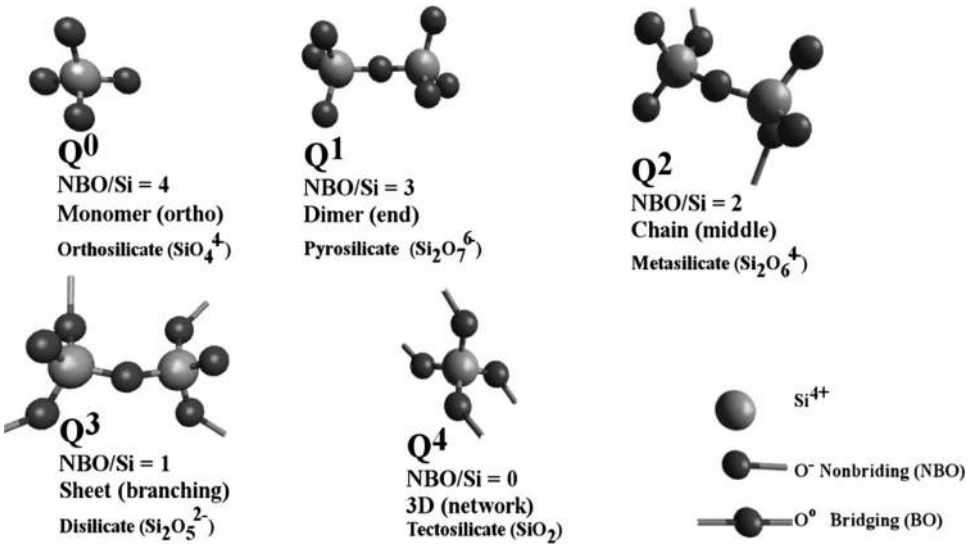

Fig. 6 Models of silicate melt structural entities with their Q-notation, NBO/Si ratios, and structural units in addition to showing the bridging oxygen (BO) and nonbridging oxygen (NBO), respectively [6, 57]

were applied to slags of interest for the Flash Ironmaking Technology (FIT), especially in terms of the effects of water vapor expected to be present in high contents in the new process [6, 55–58]. Table 1 summarizes the analysis results. The ratio of the more polymerized anions to the less polymerized anions, $(Q^2 + Q^3)/(Q^0 + Q^1)$, in the H_2O-containing atmosphere is at least twice that in the CO/CO_2 atmosphere, in agreement with the FTIR results discussed elsewhere [6, 54]. In addition, the XPS and the NBO/T suggest that the studied slag is more depolymerized under a CO/CO_2 atmosphere and more polymerized under the H_2/H_2O atmosphere [57]. It is, therefore, notable that all the results consistently lead to the conclusion that the CO/CO_2 slag has the lowest polymerization degree of all the three, whereas the two other slags have a similar degree of polymerization. This suggests that water affects the slag more significantly than CO_2 when they coexist in the gas mixture [6, 57]. Water vapor was found to be advantageous for lowering FeO in slag [46], and manganese [44]. Moreover they found that water vapor in the atmosphere of the new process would keep lining wear low based on the low MgO solubility in slag under its expected operating conditions [45]. The research on slag also found that water vapor decreased sulfur [43] and phosphorus [45] in produced molten iron.

Table 1 Comparison of a few structure analysis results [57]

Species	FTIR [6]	Raman [6]	XPS (BO, NBO)
CO/CO_2			
Q^0	59.3	28.9	11, 46
Q^1	7.0	64.4	
Q^2	33.7	6.7	
Q^3			
$(Q^0 + Q^1)/(Q^2 + Q^3)$	2.0	13.9	
$(Q^2 + Q^3)/(Q^0 + Q^1)$	0.5	0.07	
H_2/H_2O			
Q^0	18.6	53.5	17, 47
Q^1	12.7	39.0	
Q^2	15.2	7.5	
Q^3	53.5		
$(Q^0 + Q^1)/(Q^2 + Q^3)$	0.5	12.4	
$(Q^2 + Q^3)/(Q^0 + Q^1)$	2.2	0.08	
$CO/CO_2/H_2/H_2O$			
Q^0	17.9	93.5	12, 48
Q^1	29.2		
Q^2	15.4	6.5	
Q^3	37.5		
$(Q^0 + Q^1)/(Q^2 + Q^3)$	0.9	14.4	
$(Q^2 + Q^3)/(Q^0 + Q^1)$	1.1	0.07	

Economic and Environmental Aspects

A commercial scale plant flow sheet for the Flash Ironmaking Technology was constructed and its operation was simulated through detailed material and energy balance calculations [2, 4, 59, 60, 62]. Based on the process simulation, the optimum operating condition with low cost and high energy efficiency was selected. Further, an economic feasibility analysis was performed based on the process simulation results. The capital and operating costs for a commercial plant were estimated, and the net present value (NPV) after a 15 year operation was calculated. For details of the process simulation and economic analysis, the reader is referred to earlier articles from this laboratory [2, 4, 59, 60, 62].

Two potential process flow sheet configurations, the "1-step process" and "2-step process," shown in Fig. 7, were developed using hydrogen or natural gas. The main difference between the two is in the number of reactors; the reduction of magnetite to iron [reactions (6) and (7)] takes place in one reactor in the 1-step process, and it takes place in two reactors in the 2-step process. In case of hydrogen, the two steps are:

$$Fe_3O_4 + H_2 = 3FeO + H_2O(g) \quad (6)$$

$$FeO + H_2 = Fe + H_2O(g) \quad (7)$$

In the 1-step process, all materials required for producing iron are fed into the reactor, and the discharged off-gas is directly sent to heat recovery and cleaning processes for the removal of water and dusts prior to recycling the hydrogen.

The 2-step process has an iron ore pre-reduction reactor where wustite is produced. Since the reduction of wustite by hydrogen is significantly limited by equilibrium in the presence of water vapor, the off-gas from the iron producing reactor that contains a significant amount of hydrogen is used for pre-reduction of magnetite to wustite. Also, as the iron producing reactor requires a higher temperature than the pre-reduction reactor, a large amount of energy is provided in this reactor. The sensible heat contained in the off-gas from this reactor is sufficient for pre-reduction [59].

The compositions of iron ore concentrate and flux including major gangue components are given in Fig. 8. The composition of the slag after reduction reaction is also shown in Fig. 8. The slag basicity was set to be 1.2, which would provide appropriate slag viscosity to be separated from hot product iron [59]. Detailed flow sheets can be found elsewhere [2, 4, 59, 60, 62].

The hydrogen requirement was decreased by preheating the hydrogen to as high a temperature as possible by transferring the off-gas sensible heat, or decreasing the

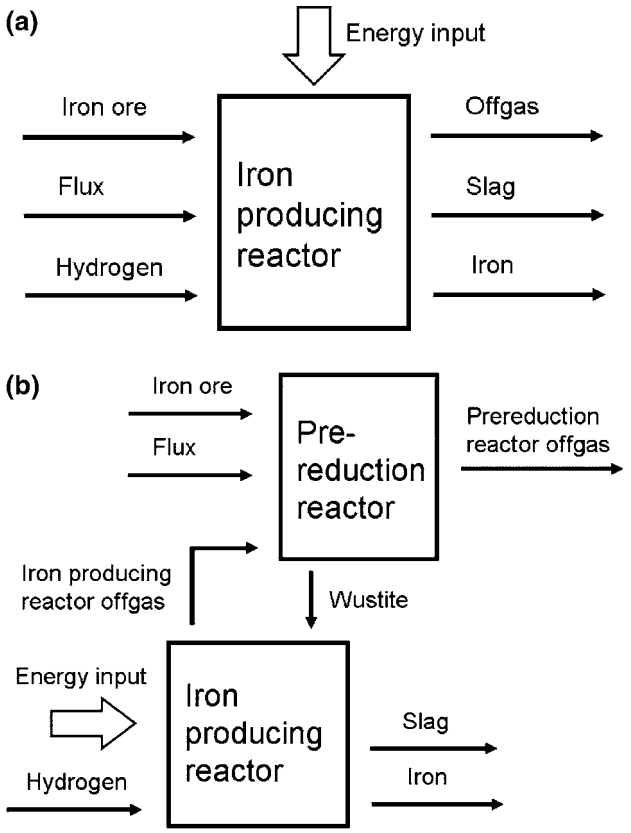

Fig. 7 Schematic diagram of iron production using hydrogen: **a** 1-step process and **b** 2-step process [59]

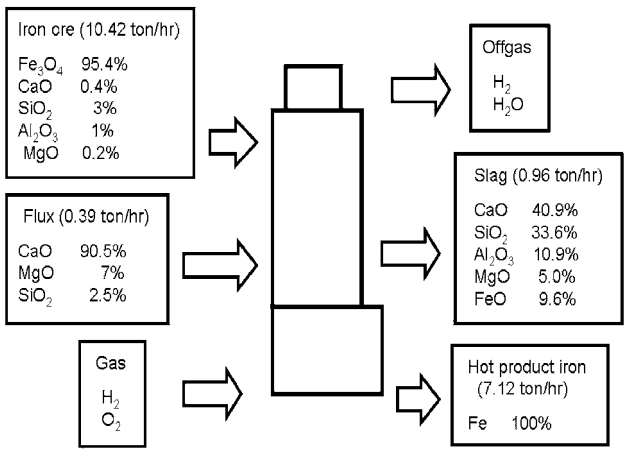

Fig. 8 Mass and composition of input and output materials around the iron producing reactor (and the pre-reduction reactor) in the pilot scale 1-step and 2-step ironmaking processes using hydrogen [59]

reactor operating temperature. Overall, the 2-step process had lower hydrogen requirement than the 1-step process. If the 1-step process would be applied, it would be critical for this process to utilize as much sensible heat of the reactor off-gas as possible for preheating hydrogen. The comparison between the 1-step and 2-step processes operated at 1500 °C and the excess driving force of 0.5 and the blast furnace process showed that both processes required less energy than the blast furnace process. However, this comparison did not include the energy required to produce purchased hydrogen [59].

An economic feasibility analysis based on "discounted cash flow analysis" was performed on the commercial scale flash ironmaking processes using natural gas or hydrogen producing one million tons of hot product iron a year. The net present value (NPV) was calculated at the discount rate of 10 % using estimated capital and operating costs for the project with 2-year construction and 15-year plant operation periods.

Process flow sheets for the commercial scale reformerless 1-step and 2-step ironmaking processes in which natural gas was directly used were constructed and simulated. The process flow sheets were constructed with hydrogen recycle, natural gas heating, a water gas shift (WGS) step, a waste heat boiler and a pressure swing adsorption step. Simulations were performed with the reactor operating at 1500 °C and an excess driving force of 0.5. The reactor feed gas preheating temperature was set to be 900 °C in the 1-step process, and 650 °C in the 2-step process. The total required energy for either reformerless process was lower than that for the blast furnace process [2, 4, 59, 60]. The results of the economic analysis indicated that the proposed "flash ironmaking process" will be economical even today if the process operates with in situ partial combustion of natural gas [62]. The total required energy for both reformerless processes was smaller than that for the blast furnace process. NPV estimation for the reformerless processes indicated that these processes would be more economic than the process using purchased hydrogen and the process combined with the steam–methane-reforming (SMR) process as will be discussed below, especially when the 1-step process was applied [2, 4, 59, 60, 62].

Process flow sheets for the commercial scale 1-step process combined with a built-in SMR step were constructed and simulated. The 1-step ironmaking process was constructed and simulated where (1) hydrogen is first produced and (2) syngas from the SMR unit is directly fed to the ironmaking unit. Simulations were performed with the reactor operating temperature of 1500 °C, the excess driving force of 0.5, and the reactor feed gas preheating temperature of 900 °C. The results showed that it would require less fresh natural gas when hydrogen was first produced and used in the iron producing reactor, which made it more economical by overcoming the additional cost of increased process steps and facilities. Also, fresh natural gas for fuel in the reformer was largely decreased by connecting the tail gas from the pressure swing adsorption (PSA) step in the ironmaking unit to the reformer burner. Compared to the blast furnace process, the

total energy required in the 1-step process combined with the SMR process was 8 % larger when hydrogen was produced and 36 % larger when syngas was produced. NPV estimation for the 1-step ironmaking process with built-in hydrogen production was estimated to be $103 million (in 2010 dollars and conditions), which benefited from the lower operating cost. Natural gas price has a large effect on NPV. CO_2 emissions credit did not affect NPV as much as the process using purchased hydrogen did [59].

In the process using purchased hydrogen, estimated NPV was negative $475 million (in terms of 2010 dollars and conditions) in the 1-step process, and negative $530 million (in 2010 dollars and conditions) in the 2-step process, respectively. However, the 1-step process could be economic depending on the availability of less-expensive hydrogen, CO_2 emissions credit trading, and the price of iron [59].

These results indicate that the proposed "flash ironmaking process" will be economical even today if the process operates with in situ partial combustion of natural gas. Major results are summarized in Figs. 9 and 10. Figure 9 shows potential energy saving, lower carbon footprint, and economic feasibility (except when purchased H_2 is used) relative to the BF. However, application of a $50 per ton of CO_2 credit should make the use of hydrogen economically feasible at the 2010 price of hydrogen, as Fig. 10 indicates [4, 60, 62]. The values of CO_2 emissions

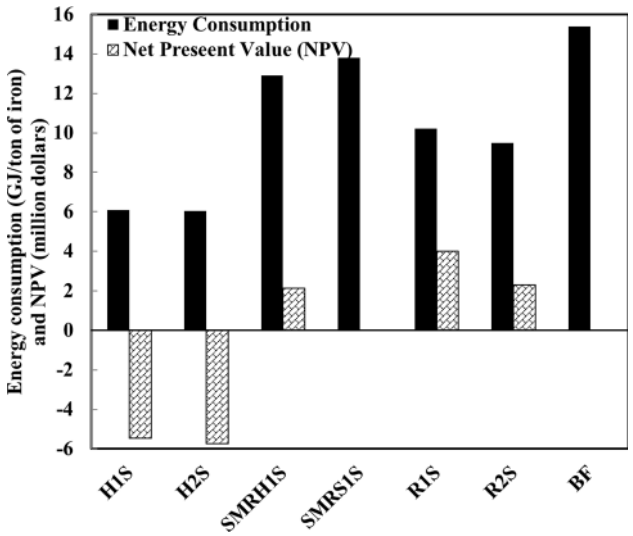

Fig. 9 Energy consumption (GJ/ton of iron) and NPV (million dollars, relative to 2010 dollars and conditions using $2.5/kg for hydrogen, and $6/million Btu for natural gas) applying $0 CO_2 credit for a 1 Mt/year plant of different configurations of the Flash Ironmaking Technology compared with average blast furnace. (H1S: H_2-based 1-step process, H2S: H_2-based 2-step process, SMRH1S: 1-step process with hydrogen production from SMR (Steam-Methane Reforming), SMRS1S: 1-step process with syngas production from SMR, R1S: Reformerless1-step process, R2S: Reformerless 2-step process) [4, 60, 62]

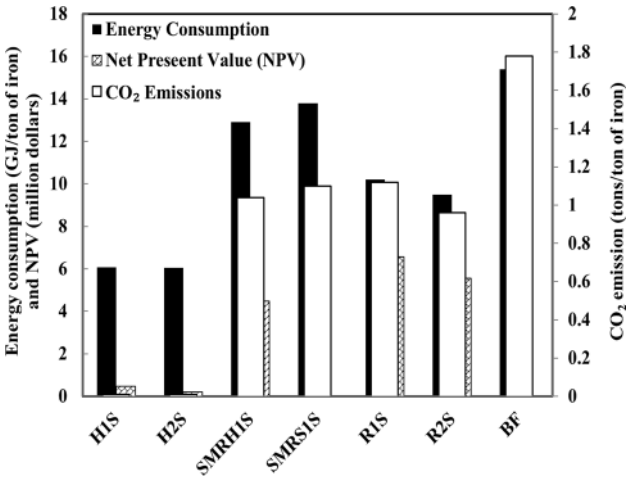

Fig. 10 The energy consumption (GJ/ton of iron), NPV (million dollars, irelative to 2010 dollars and conditions using $2.5/kg for hydrogen, and $6/million Btu for natural gas) applying $50 CO_2 credit, and CO_2 emissions (tons/ton of iron) for a 1 Mt/year plant of different configurations of the Flash Ironmaking Technology compared with average blast furnace [4, 60, 62]

for the hydrogen-based flash ironmaking processes assume only those from limestone calcination and none from the ironmaking step. It is recognized that hydrogen production may involve CO_2 generation, but since there are many possible methods of its production with varying degrees of CO_2 emissions, including the reforming of natural gas or biomass or the electrolysis of water using nuclear or solar energy, the carbon footprint of hydrogen production was not considered in this analysis.

This transformative technology has significant energy saving and reduced CO_2 emissions compared with the Blast Furnace process. It has been proved that iron particles of more than 95 % metallization can be obtained by reduction with hydrogen or a mixture of carbon monoxide and hydrogen in 2–7 s at temperatures of 1573 K (1300 °C) or above. The product of Flash Ironmaking Technology (FIT), which is expected to operate at temperatures higher than 1273 K (1000 °C), is significantly less reactive toward oxygen compared with DRI produced by the current technologies. Also, the molten iron produced by the FIT will contain less impurities and the relevant slag would be less corrosive to furnace lining.

Conclusions

The Flash Ironmaking Technology (FIT) was conceived as a novel ironmaking process at the University of Utah. This technology is based on fine particle reduction using a reductant gas such as hydrogen, natural gas, coal gas, or a combination thereof. It is the first flash-type ironmaking process converting iron ore concentrates directly to

metallic iron in-flight, which would be suitable for an industrial-scale operation. This process will produce iron without requiring pelletization or sintering of iron ore and also avoids the need for coke. In addition, this process concept takes full advantage of the fine particle size of the concentrate with a large surface area, which permits rapid reduction by a gas. Another potential benefit of this process is the possibility of steelmaking in a single, continuous process. This transformative technology is expected to allow significant energy saving and reduced CO_2 emissions compared with the Blast Furnace process.

Acknowledgments The authors acknowledge the financial support from the American Iron and Steel Institute (AISI) through a Research Service Agreement with the University of Utah under the AISI's CO_2 Breakthrough Program. This article also contains results of work supported by the U.S. Department of Energy under Award Number DE-EE0005751.

References

1. Choi ME, Sohn HY (2010) Development of green suspension ironmaking technology based on hydrogen reduction of iron oxide concentrate: rate measurements. Ironmak Steelmak 37(2):81–88
2. Pinegar HK, Moats MS, Sohn HY (2011) Process simulation and economic feasibility analysis for a hydrogen-based novel suspension ironmaking technology. Steel Res Int 82(8):951–963
3. Mohassab-Ahmed MY, Sohn HY, Kim HG (2012) Sulfur distribution between liquid iron and magnesia-saturated slag in H_2/H_2O atmosphere relevant to a novel green ironmaking technology. Ind Eng Chem Res 51(9):3639–3645
4. Pinegar H, Moats M, Sohn HY (2012) Flowsheet development, process simulation and economic feasibility analysis for novel suspension ironmaking technology based on natural gas: part 1-Flowsheet and simulation for ironmaking with reformerless natural gas. Ironmak Steelmak 39(6):398–408
5. Sohn HY (2007) Suspension ironmaking technology with greatly reduced energy requirement and CO_2 emissions. Steel Times Int 31(4):68–72
6. Mohassab Ahmed MY, Phase equilibria between iron and slag in $CO/CO_2/H_2/H_2O$ atmospheres relevant to a novel flash ironmaking technology, in metallurgical engineering. 2013, PhD dissertation, The University of Utah, Salt Lake City, Utah, USA
7. Mohassab-Ahmed MY, Sohn HY, Kim HG (2012) Phosphorus distribution between liquid iron and magnesia-saturated slag in H_2/H_2O atmosphere relevant to a novel ironmaking technology. Ind Eng Chem Res 51(20):7028–7034
8. Cheeley R (1999) Gasification and the midrex direct reduction process. In: Gasification technologies conference, San Francisco, CA
9. Duarte PE, Becerra J, Lizcano C, Martinis A (2008) ENERGIRON direct reduction technology-economical, flexible, environmentally friendly. Acero LatinoAm 6:52–58
10. Hassan A, Whipp R, Millionis K, Zeller S (1994) Development of an improved fluid bed reduction process. In: Ironmaking conference proceedings, Iron and Steel Society of AIME, Warrendale, PA, pp 481–490
11. Husain R, Sneyd S, Weber P (1999) Circored and Circofer—two new fine ore reduction processes. In: Publ. Australas. Inst. Min. Metall. 3/99, ICARISM '99, Proceedings of the International Conference on Alternative Routes of Iron and Steelmaking (Carlton South, VIC, Australia: Australian Institute of Mining and Metallurgy), pp 123–129
12. Macauley D (1997) Options increase for non-BF ironmaking. Steel Times Int 21(1):20
13. Ray HS, Kundu N (1986) Thermal analysis studies on the initial stages of iron oxide reduction. Thermochim Acta 101:107–118
14. Edstrom JO (1953) The mechanism of reduction of iron oxides. J Iron Steel Inst 175:289–304
15. Srinivasan MV, Sheasby JS (1981) A study of the reduction of hematite to magnetite using a stabilized zirconia cell. Metall Trans B 12B(1):177–185
16. Piotrowski K, Mondal K, Wiltowski T, Dydo P, Rizeg G (2007) Topochemical approach of kinetics of the reduction of hematite to wüstite. Chem Eng J 131(1–3):73–82
17. Sturn J, Voglsam S, Weiss B, Schenk J, Winter F (2009) Evaluation of the limiting regime in iron ore fines reduction with H_2-rich gases in fluidized beds: Fe_2O_3 to Fe_3O_4. Chem Eng Technol 32(3):392–397
18. Fruehan RJ, Li Y, Brabie L, Kim EJ (2005) Final stage of reduction of iron ores by hydrogen. Scand J Metall 34(3): 205–212
19. Monazam ER, Breault RW, Siriwardane R (2014) Kinetics of hematite to wüstite by hydrogen for chemical looping combustion. Energy Fuels 28(8):5406–5414
20. Wang H, Sohn HY (2013) Hydrogen reduction kinetics of magnetite concentrate particles relevant to a novel flash ironmaking process. Metall Mater Trans B 44(1):133–145
21. Choi ME, Sohn HY, Han G (2006) The kinetics of hydrogen reduction of fine iron oxide particles. In: Kongoli F, Reddy RG (eds) Sohn international symposium advanced processing of metals and materials, vol 2—thermo and physicochemical principles: iron and steel making. TMS, Warrendale, PA, pp 105–110
22. Chen F, Mohassab Y, Zhang S, Sohn HY (2015) Kinetics of the reduction of hematite concentrate particles by carbon monoxide relevant to a novel flash ironmaking process. Metall Mater Trans B 46B(4):1716–1728
23. Chen F, Mohassab Y, Jiang T, Sohn HY (2015) Hydrogen reduction kinetics of hematite concentrate particles relevant to a novel flash ironmaking process. Metall Mater Trans B 46(3): 1133–1145
24. Avrami M (1939) Kinetics of phase change. I General theory. J Chem Phys 7(12):1103–1112
25. Avrami M (1940) Kinetics of phase change. II. Transformation-time relations for random distribution of nuclei. J Chem Phys 8(2):212–224
26. Avrami M (1941) Granulation, phase change, and microstructure kinetics of phase change. III. J Chem Phys 9(2):177–184
27. Mohassab Y, Chen F, Elzohiery M, Abelghany A, Zhang S, Sohn HY (2016) Reduction kinetics of hematite concentrate particles by $CO + H_2$ mixture relevant to a novel flash ironmaking process. In: 7th international symposium on high temperature metallurgical processing, TMS, Warrendale, PA and John Wiley & Sons, Hoboken, NJ, pp 35–40
28. Yuan Z, Sohn HY (2014) Re-oxidation kinetics of flash reduced iron particles in O_2–N_2 gas mixtures relevant to a novel flash ironmaking process. ISIJ Int 54(6):1235–1243
29. Yuan Z, Sohn HY, Olivas-Martinez M (2013) Re-oxidation kinetics of flash-reduced iron particles in H_2–H_2O(g) atmosphere relevant to a novel flash ironmaking process. Metall Mater Trans B 44(6):1520–1530
30. Yuan Z (2013) Re-oxidation kinetics of flash-reduced iron particles relevant to a novel flash ironmaking process. M.S. Thesis, The University of Utah, Salt Lake City, Utah, USA
31. Tomlinson JW (1956) A note on the solubility of water in a molten sodium silicate. J Soc Glass Technol 40:25T–31T

32. Schwerdtfeger K, Schubert HG (1978) Solubility of water in $CaO–Al_2O_3$ melts at 1600°C. Metall Trans B 9B(1):143–144
33. Russell LE (1957) Solubility of water in molten glass. J Soc Glass Technol 41:304T–317T
34. Pelton AD (1999) Thermodynamic calculations of chemical solubilities of gases in oxide melts and glasses. Glass Sci Technol 72(7):214–226
35. Mysen BO, Virgo D, Harrison WJ, ScARFE CM (1980) Solubility mechanisms of H_2O in silicate melts at high pressures and temperatures: a Raman spectroscopic study. Am Mineral 65(9–10):900–914
36. Mysen BO (1990) Interaction between water and melt in the system calcium aluminate–silica–water. Chem Geol 88(3–4):223–243
37. Iguchi Y, Fuwa T (1970) Solubility of water in liquid $CaO–SiO_2–MgO$ with and without "FeO" at 1550 °C. Trans Iron Steel Inst Jpn 10:29–35
38. Iguchi Y, Ban-Ya S, Fuwa T (1969) Solubility of water in liquid $CaO–SiO_2$ with Al_2O_3, TiO_2, and FeO at 1500 °C. Trans Iron Steel Inst Jpn 9:189–195
39. Brandberg J, Sichen D (2006) Water vapor solubility in ladle-refining slags. Metall Trans B 37(3):389–393
40. Zuliani DJ, Iwase M, McLean A (1982) The thermodynamics of water vapor dissolution in $CaO–MgO–SiO_2$ slags. Trans Iron Steel Soc AIME 1:61–67
41. Sosinsky DJ, Maeda M, McLean A (1985) Determination and prediction of water vapor solubilities in $CaO–MgO–SiO_2$ slags. Metall Trans B 16B(1):61–66
42. Mohassab-Ahmed MY, Sohn HY (2014) Effect of water on S and P distribution between liquid Fe and MgO-saturated slag relevant to a flash ironmaking technology. In: Yurko J et al. (eds) EPD congress. TMS, Warrendale, PA and John Wiley & Sons, Hoboken, NJ, pp 203–210
43. Mohassab Y, Sohn HY (2014) Effect of water vapor on sulfur distribution between liquid Fe and MgO-saturated slag relevant to a flash ironmaking technology. Steel Res Int 86(7):753–759
44. Mohassab-Ahmed MY, Sohn HY (2014) Effect of water vapor content in $H_2–H_2O–CO–CO_2$ mixtures on the equilibrium distribution of manganese between $CaO–MgO_{sat}–SiO_2–Al_2O_3–FeO–P_2O_5$ slag and molten iron. Steel Res Int 85(5):875–884
45. Mohassab-Ahmed MY, Sohn HY, Zhu L (2014) Effect of water vapour content in $H_2–H_2O–CO–CO_2$ mixtures on MgO solubility in slag under conditions of novel flash ironmaking technology. Ironmak Steelmak 41(8):575–582
46. Mohassab-Ahmed MY, Sohn HY (2014) Effect of Water Vapor Content in $H_2–H_2O–CO–CO_2$ mixtures on the activity of iron oxide in slags relevant to a novel flash ironmaking technology. Ironmak Steelmak 41(9):665–675
47. Stevels JM (1954) Networks in glasses and other polymers. Glass Ind 35:657–662
48. Masson C (1984) The chemistry of slags—an overview. In: Fine HA, Gaskell DR (eds) Proceedings on 2nd international symposium metallurgical slags fluxes. TMS, Warrendale, PA, pp. 3–44
49. Mills K (1995) Slag atlas. Verlag Stahleisen GmbH, Düsseldorf
50. Huggins ML (1954) The structure of amorphous materials. J Phys Chem 58(12):1141–1146
51. Fraser DG (1977) Thermodynamic properties of silicate melts. Thermodyn Geol 30:301–325
52. Živković Ž, Mitevska N, Mihajlović I, Nikolić Đ (2009) The influence of the silicate slag composition on copper losses during smelting of the sulfide concentrates. J Mining Metall B Metall 45(1):23–34
53. Mills K (1991) The structure of silicate melts. National Physical Laboratory, Division of Materials Applications (DMA), Teddington
54. Mohassab Y, Sohn HY (2014) Analysis of slag chemistry by FTIR-RAS and Raman spectroscopy: effect of water vapor content in $H_2–H_2O–CO–CO_2$ mixtures relevant to a novel green ironmaking technology. Steel Res Int 86(7):740–752
55. Mohassab-Ahmed MY, Sohn HY (2013) Application of spectroscopic analysis techniques to the determination of slag structures and properties: effect of water vapor on slag chemistry relevant to a novel flash ironmaking technology. JOM 65(11): 1559–1565
56. Mohassab Y, Sohn HY (2015) Effect of water vapor on O^{2-} content in ironmaking slag. J Iron Steel Res Int 22(10):909–915
57. Mohassab Y, Sohn HY, Devener BV (2015) An X-ray photoelectron spectroscopy (XPS) study of the effect of water vapor on slag chemistry and structure related to a novel flash ironmaking process: part 1—experimental work. AIST Trans 12(8):179–186
58. Mohassab Y, Sohn HY (2015) An X-ray photoelectron spectroscopy (XPS) study of the effect of water vapor on slag chemistry and structure related to a novel flash ironmaking process: part 2—calculation of the degree of polymerization. AIST Trans 12(9):185–191
59. Kimura H (2010) Material and energy flow simulation and economic analysis for a novel suspension ironmaking techonology. MS thesis, The University of Utah, Salt Lake City, UT
60. Pinegar HK, Moats MS, Sohn HY (2013) Flowsheet development, process simulation and economic feasibility analysis for novel suspension ironmaking technology based on natural gas: part 2—Flowsheet and simulation for ironmaking combined with steam methane reforming. Ironmak Steelmak 40:32–43
61. Sohn HY, Choi ME (2012) Steel industry and carbon dioxide emissions—a novel ironmaking process with greatly reduced carbon footprint. In: Carpenter M, Shelton EJ (eds) Carbon dioxide emissions: new research. Nova Science Publishers Inc, Hauppauge
62. Pinegar HK, Moats MS, Sohn HY (2013) Flowsheet development, process simulation and economic feasibility analysis for novel suspension ironmaking technology based on natural gas: part 3—Economic feasibility analysis. Ironmak Steelmak 40: 44–49